CONDENSED MATTER PHYSICS

Coherent order parameter oscillations in the ground state of the excitonic insulator Ta_2NiSe_5

Daniel Werdehausen,[1,2]* Tomohiro Takayama,[1,3] Marc Höppner,[1†] Gelon Albrecht,[1,2] Andreas W. Rost,[1,3‡] Yangfan Lu,[4] Dirk Manske,[1] Hidenori Takagi,[1,3,4] Stefan Kaiser[1,2§]

The excitonic insulator is an intriguing electronic phase of condensed excitons. A prominent candidate is the small bandgap semiconductor Ta_2NiSe_5, in which excitons are believed to undergo a Bose-Einstein condensation–like transition. However, direct experimental evidence for the existence of a coherent condensate in this material is still missing. A direct fingerprint of such a state would be the observation of its collective modes, which are equivalent to the Higgs and Goldstone modes in superconductors. We report evidence for the existence of a coherent amplitude response in the excitonic insulator phase of Ta_2NiSe_5. Using nonlinear excitations with short laser pulses, we identify a phonon-coupled state of the condensate that can be understood as a novel amplitude mode. The condensate density contribution substantiates the picture of an electronically driven phase transition and characterizes the transient order parameter of the excitonic insulator as a function of temperature and excitation density.

INTRODUCTION

Excitonic insulators (EIs) are expected in semimetals with a small band overlap or small bandgap semiconductors (*1*–*5*). In semiconductors, a Bose-Einstein–like condensation of preformed excitons can occur if their binding energy exceeds the bandgap, whereas semimetals undergo a Bardeen-Cooper-Schrieffer (BCS)–like transition (*6*). A characteristic spectroscopic fingerprint of this transition is a band flattening, which can be observed in angle-resolved photoemission spectroscopy (ARPES) measurements (*7*–*9*). By itself, however, this cannot elucidate the microscopic origin of the gap of a potential EI. For this purpose, ultrafast methods provide the possibility to gain further insight. Gap melting times observed in time-resolved ARPES (tr-ARPES) measurements were used to distinguish Mott-, exciton-, and lattice-driven dynamics (*10*, *11*). In particular, for the charge density wave (CDW) and the excitonic order in $TiSe_2$, a combination of tr-ARPES (*11*, *12*), x-ray (*13*), electron diffraction (*14*), and terahertz pulses (*15*) allows tracking of the complicated interplay of electronic interactions and lattice distortions that drive the phase transition. Furthermore, time-domain spectroscopy also offers a way to directly identify a symmetry-broken state. This can be achieved by probing the state's collective excitations, namely, the amplitude (*16*–*21*) and the phase mode (*22*, *23*). Probing the amplitude mode offers the possibility to map out the transient state's order parameter as a function of temperature and excitation density. For electronically driven transitions, these measurements reveal a characteristic behavior of the electronic Higgs mode that allows distinguishing it from impulsively excited coherent phonons.

Here, we study the collective excitations in Ta_2NiSe_5, a potential EI, to prove the existence of a coherent condensate. In doing so, we identified a low-frequency phonon that, under nonlinear excitation, directly couples to the excitonic condensate. This coupling arises from the quasi–one-dimensional (1D) structure of Ta_2NiSe_5, which consists of Ni and Ta chains aligned along the *a* axis (Fig. 1A). Recent ARPES measurements showed that the valence band flattening, characteristic of the EI transition, occurs below 328 K (*7*, *8*, *24*, *25*). This is accompanied by a structural transition from an orthorhombic to a monoclinic crystal system, where the slight distortion does not result in the formation of a CDW (*24*, *26*). Numerical calculations have shown that the band flattening and the structural transition can be attributed to the formation of excitons between Ta 5d electrons and hybridized Ni 3d–Se 4p holes (*24*). An illustration of a charge transfer exciton in the material is shown in Fig. 1B: A completely filled valence band corresponds to a double occupancy of each Ni site. An exciton is formed if an electron hops to the conduction band, supplied by the Ta chains, and binds to the hole it left behind on the Ni chain. This spatial separation of the electrons from the holes prevents recombination and is believed to be the reason for the stable exciton states in the material (*26*, *27*). The consequence of the exciton formation and their Bose-Einstein–like condensation is the opening of a large gap (Δ_{EI} = 160 meV) (*25*–*27*). Recent tr-ARPES probed the photodoping dynamics of this gap and found that, beyond a certain threshold fluence, the gap becomes transiently enhanced on a time scale of about 200 fs (*28*). That behavior, opposite to a bandgap narrowing, as expected for semiconductors, was explained on the basis of Hartree-Fock calculations by an enhancement of the EI order parameter. Because the size of the gap directly denotes the frequency of the excitonic condensate's expected Higgs mode equivalent, it has a period (τ_Δ) of about $\tau_\Delta = h/\Delta = 26$ fs. In real space, this amplitude oscillation of the order parameter corresponds to a collective hopping of electrons and holes between the Ta and Ni chains (gray lines in Fig. 1B). However, it has been predicted recently that in the presence of strong electron-phonon coupling, a superconducting order parameter can also couple to a phonon, thus forming a new amplitude mode, which consists of intertwined lattice and order parameter oscillations (*29*). Although on completely different energy scales as for the strongly electron-phonon–coupled superconductor, as described by Murakami *et al.* (*29*), here, we report on strong experimental evidence for the existence of such a coupled amplitude mode in Ta_2NiSe_5. This new collective mode is distinguished from normal coherent phonons by its temperature and excitation density dependence. Its mode amplitude traces the behavior that would be expected for the purely electronic amplitude (Higgs) mode. This enables us to map out the order parameter as a function of temperature and excitation density.

[1]Max Planck Institute for Solid State Research, 70569 Stuttgart, Germany. [2]4th Physics Institute, University of Stuttgart, 70569 Stuttgart, Germany. [3]Institute for Functional Matter and Quantum Technologies, University of Stuttgart, 70569 Stuttgart, Germany. [4]Department of Physics, The University of Tokyo, Bunkyo-ku, Tokyo 113-0033, Japan.
*Present address: Carl Zeiss AG, Corporate Research and Technology, Carl-Zeiss-Promenade 10, 07745 Jena, Germany.
†Present address: QuantumWise A/S (part of Synopsys), Fruebjergvej 3, DK-2100 Copenhagen, Denmark.
‡Present address: Scottish Universities Physics Alliance, School of Physics and Astronomy, University of St Andrews, North Haugh, St Andrews, Fife KY16 9SS, UK.
§Corresponding author. Email: s.kaiser@fkf.mpg.de

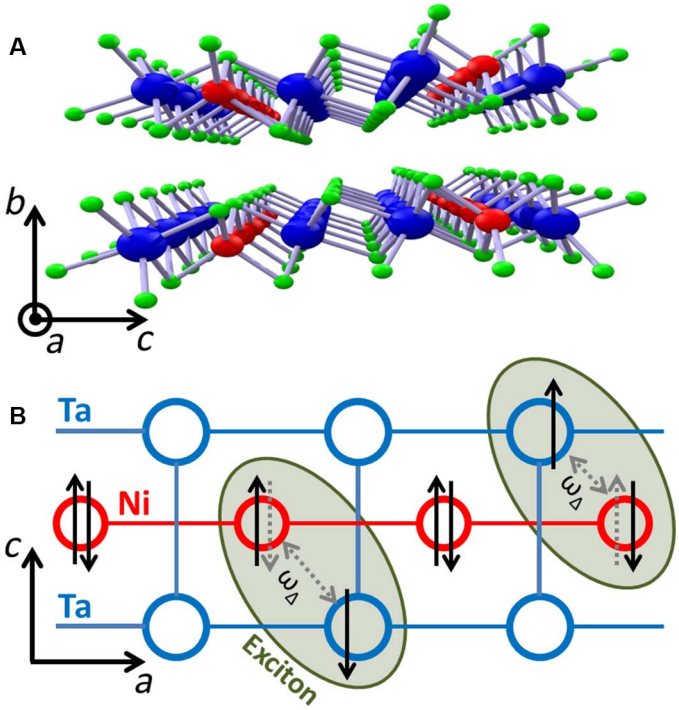

Fig. 1. Structure of Ta_2NiSe_5. (**A**) The Ni (red) and Ta (blue) 1D chains are aligned along the *a* axis and forming sheets in the *ac* plane. The electronic transport forms along the chains in *a* direction (Se atoms are marked green). (**B**) Structure and exciton formation along the chains: The Ni chains supply the valence band, and the Ta chains supply the conduction band. In the semiconducting phase, all Ni sites are doubly occupied. An exciton is formed between an electron on the Ta chains and a hole on the Ni chain. The Higgs amplitude mode (frequency ω_Δ) corresponds to a collective hopping of electrons and holes between the chains.

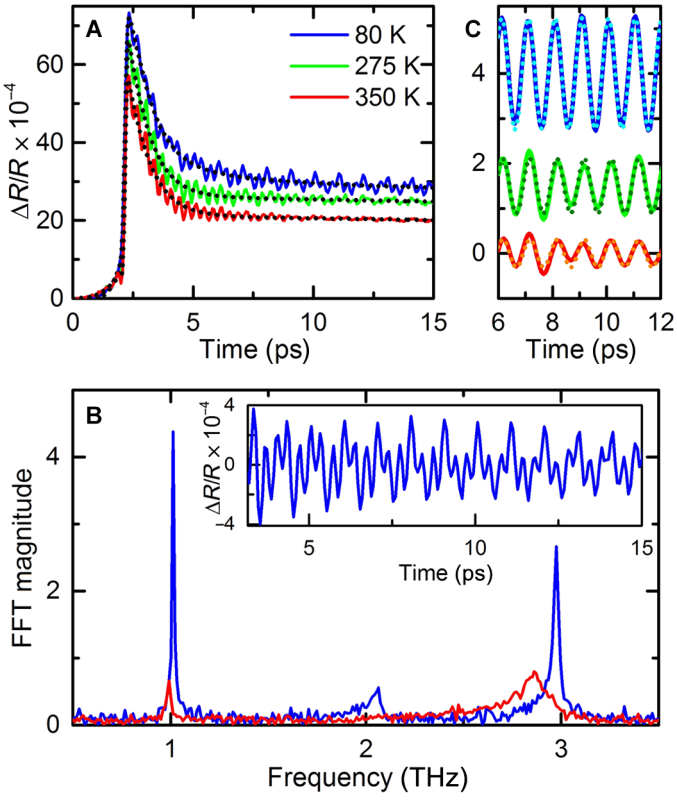

Fig. 2. Pump-robe response. (**A**) Time trace of photoinduced reflectivity changes at different temperatures and an excitation density of 0.35 mJ/cm^2. The signal is made up of the electronic response and the coherent oscillations. The dotted black lines represent fits to the measured data. (**B**) The inset shows only the coherent oscillations, which were extracted by substracting the fits in (A) from the measured data. The main panel of (B) presents the corresponding FFTs at 80 and 350 K. (**C**) Phonon-coupled amplitude mode at 1 THz, which was extracted using an FFT band-pass filter. The amplitude (A_{EI}) of the coupled mode was determined by fitting a damped harmonic oscillator to the data (dotted lines).

RESULTS

To investigate the collective excitations of Ta_2NiSe_5, we performed pump-probe experiments using 1.55-eV (800 nm), 130-fs laser pulses. We probe the system's coherent oscillations below and above the critical temperature to characterize the temperature and excitation density dependence of their potential coupling to the excitonic condensate. To excite the modes without depleting the condensate significantly, we performed the experiments at perpendicular polarization to the chains. In the case of parallel polarization, the coupling of the light pulses to the condensate is enhanced. In this configuration, a complete depletion of the condensate occurs even at low excitation densities (see the Supplementary Materials).

Figure 2A depicts the time dependence of the photoinduced reflectivity changes $\Delta R/R(t)$ at perpendicular polarization to the chains at different temperatures. The measured time trace is a superposition of the electronic signal and several coherent oscillations. The electronic part describes the photodoping and exciton-breaking dynamics into electrons and holes and their subsequent recombination in agreement with the photodoping dynamics found in the tr-ARPES experiments (*28*). It consists of a steep onset (time constants, ~0.1 and ~1 ps) and a double-exponential decay (time scales, ~1 and ~10 ps). The coherent oscillations on top of the electronic signal are made up of one mode at ~1 THz that we find to be coupled to the EI (see Discussion) and two coherent phonons at higher frequencies, which were excited via impulsive stimulated Raman scattering (*30*). To extract the coherent oscillations, we subtracted the fit to the electronic background (dotted black lines) from the measured signal. This yielded the oscillations shown in the inset of Fig. 2B. The corresponding fast Fourier transforms (FFTs) at 80 and 350 K are presented in the main panel of Fig. 2B. It can be seen that at 80 K, the spectrum contains three distinct modes at 1.01, 2.07, and 2.98 THz (from here on denoted as 1-, 2-, and 3-THz modes). Using local density approximation (LDA) calculations and Raman measurements (see the Supplementary Materials), the 1-THz oscillation was identified as an A_{1g} mode, whereas the 2-THz (3-THz) mode is a B_{1g} (A_{1g}) phonon. Comparing the FFTs at the different temperatures reveals that, upon heating, a significant decrease in the peak height occurs for both the 1- and 3-THz modes, whereas the 2-THz mode becomes heavily damped and disappears completely. To investigate the behavior of the modes quantitatively, we applied FFT band-pass filters with a bandwidth of 1 THz around the respective peaks. The results for the 1-THz mode, which are depicted in Fig. 2C, show a decrease of the amplitude with increasing temperature. To investigate this dependency systematically, we determined the initial oscillation amplitude $A_{EI} = \Delta R_{1THz}/R(t = 0)$ by fitting a damped harmonic oscillator to the data.

Measuring A_{EI} as a function of temperature and excitation density reveals that the 1-THz mode is indeed coupled to the excitonic condensate. The behavior of an uncoupled coherent phonon is presented, for comparison, on the example of the 3-THz mode. Figure 3A depicts A_{EI}

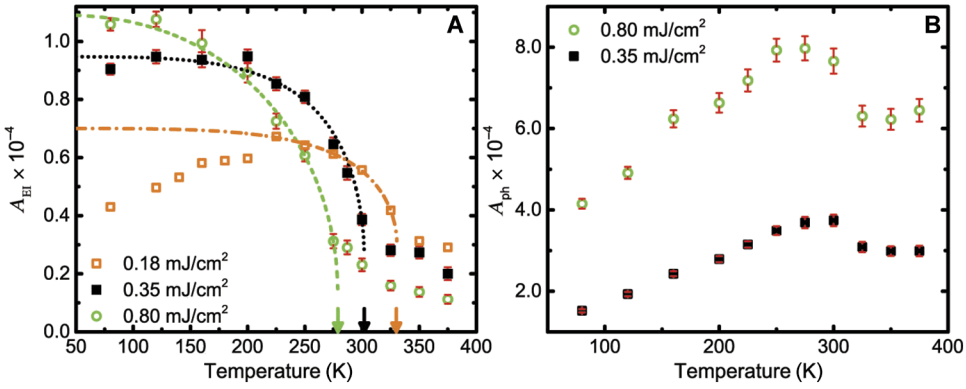

Fig. 3. Temperature dependence. (**A**) Amplitude of the coupled mode (A_{EI}) at 1 THz over temperatures at different excitation densities. The fits (dotted and dashed lines) denote a mean field-like order parameter that was fitted to the low-temperature data points. For the measurement at 0.18 mJ/cm^2, only points above 225 K were used for the fit. The arrows illustrate the position of T_C at the respective excitation density. (**B**) Amplitude of the uncoupled phonon mode (A_{ph}) at 3 THz over temperatures at different excitation densities.

as a function of temperature at different excitation densities. At the two highest excitation densities, the amplitude remains almost constant at low temperatures. However, upon increasing the temperature, the amplitude decreases with a behavior that is reminiscent of a typical mean field order parameter. The temperature dependence is completely different for normal coherent phonons in semiconductors, which show a behavior that is similar to the uncoupled phonon mode at 3 THz (Fig. 3B) or the equivalent noncoupled 1.2-THz phonon in Ta_2NiS_5 (see the Supplementary Materials). Figure 3B shows, on the example of the 3-THz mode, that the amplitudes of these modes increase with increasing temperature. To show that the amplitude of the 1-THz mode in Ta_2NiSe_5 (A_{EI}) indeed follows an order parameter behavior at a fixed excitation density, we fitted a BCS-type interpolation formula, which is also valid for the EI (*5*), to the low-temperature data: $\Delta(T) = \Delta(0)\tanh\left(\beta\sqrt{\frac{T_c}{T}-1}\right)$ (*31*), where T_c denotes the critical temperature. Except for the excitation density–dependent shift of the critical temperature to lower temperatures, this behavior is in agreement with the temperature dependence of the order parameter extracted from ARPES measurements and variational cluster approximation calculations (*25*). This directly underpins the coupling of the 1-THz mode to the EI state. At temperatures above T_c, the amplitude deviates from the order parameter behavior and levels off into a regime, in which the amplitude only changes slowly but remains finite. This can be attributed to strong fluctuations, which are expected in the Bose-Einstein condensation (BEC)–like regime of the EI phase (*6*, *8*) and which were also observed in ARPES measurements (*25*). Another fact for the enhanced oscillation amplitudes could arise because of a shallower phonon potential of the EI-phonon–coupled mode (see Discussion) at elevated temperatures that becomes more dominant in the presence of order parameter fluctuations. In the Supplementary Materials, we show that at parallel polarization to the chains, it is possible to completely deplete the condensate, which can be seen from a complete elimination of the 1-THz mode ($A_{EI} = 0$). At the excitation density of 0.35 mJ/cm^2 (0.8 mJ/cm^2), the fit ansatz yielded a T_c of 302 K (279 K). The deviation of T_c from the equilibrium value of 328 K obtained from transport and ARPES measurements (*25*) can be attributed to the pump pulses, which break a certain number of excitons and hence deplete the EI. Because the amount of optical depletion increases with increasing power, this also explains the shift of T_c to lower temperatures with increasing excitation density. In contrast, in the low-temperature regime, where thermal depletion does not play a role, stronger pump pulses lead to a greater excitation of the coupled exciton-phonon system and, therefore, to a higher amplitude.

To determine the behavior of the coupling closer to equilibrium conditions, we investigated the temperature dependence also at a lower excitation density. The results, which are also depicted in Fig. 3A, show that in this case, the amplitude of the 1-THz mode only follows the order parameter at temperatures above 225 K. The corresponding fit yielded a T_c of 330 K, which, as expected for the low-power case, agrees well with the equilibrium value of 328 K. In the low-temperature regime, however, the amplitude of the 1-THz mode deviates from the order parameter behavior, and instead of a constant value, an increase of the amplitude with increasing temperature is seen. The 1-THz mode's linear Raman response (see the Supplementary Materials) and the temperature dependence of the 3-THz coherent phonon (Fig. 3B) show that this is the behavior of an uncoupled coherent phonon. The fact that the 1-THz mode behaves like an uncoupled phonon at low excitation densities indicates that there is an excitation threshold that has to be overcome to reach the nonlinear excitation regime, in which the condensates coupling to the phonon become exposed. This threshold is temperature-dependent: At low temperatures, the EI is trapped in a deep potential, and therefore, a high excitation density is needed to overcome the threshold. However, at higher temperatures, the thermal depletion of the excitonic condensate lowers the potential barrier, and lower excitation densities are consequently sufficient to drive the excitonic system into the highly nonlinear regime, exposing the coupling to the phonon mode. In the Supplementary Materials, we show that, even at lower excitation densities, the coupling remains inefficient over the entire temperature range and that the lack of coupling in these cases is also confirmed by the temperature dependence of the mode's frequency. In the coupled case, however, the amplitude A_{EI} follows the order parameter of the EI.

To further elaborate on the threshold behavior and characterize the excitation density dependence of the order parameter, we carried out excitation fluence–dependent measurements at two different temperatures: (i) at 120 K, that is, deep inside the EI phase, and (ii) at 250 K, that is, in a regime where thermal excitation of the condensate sets in (Fig. 4A). Both measurements show qualitatively the same behavior: At low excitation densities (shaded area), a steep onset is observed. In this regime, the amplitude is proportional to the square root of the pump power, that is, proportional to the electric field. With increasing power, the amplitude deviates from this simple behavior, reaches a maximum, and decreases roughly linearly when the excitation density is further increased. As discussed below, this power dependence is a direct consequence of the

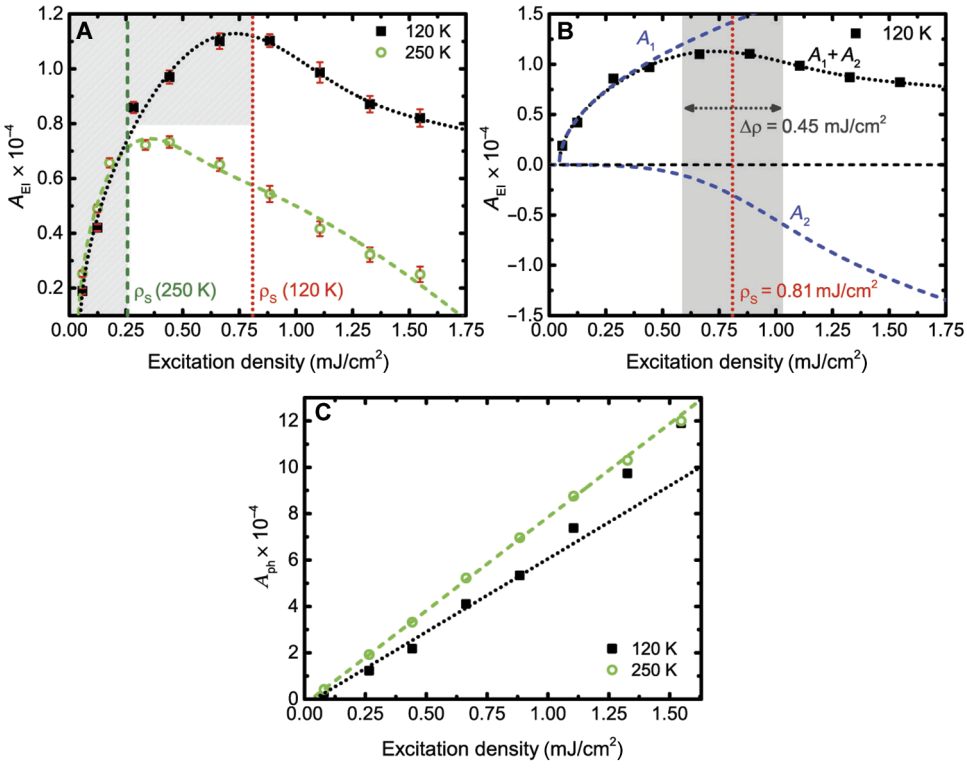

Fig. 4. Fluence dependence. (**A**) Amplitude of the coupled mode (A_{EI}) at 1 THz over excitation density at 120 and 250 K. As discussed in the main text, the fit (dotted and dashed lines) reveals the threshold (ρ_s) that characterizes the onset of the coupling to the excitonic condensate. The shaded area indicates the regime in which the coupling of the condensate to the phonon is not effective. (**B**) Separate fit components (A_1 and A_2) for the measurement at 120 K. The shaded area describes the width of the step function, which characterizes the threshold. (**C**) Amplitude of the uncoupled phonon mode (A_{ph}) at 3 THz over excitation density at 120 and 250 K.

coupling of the 1-THz phonon to the excitonic condensate. In contrast, the 3-THz mode's amplitude (see Fig. 4C) increases linearly with power over the entire range, as expected for a coherent phonon (*32*–*35*). The fits to the 1-THz mode's amplitude in Fig. 4 were accordingly constructed as a sum of the two components: a square root increase (component A_1) and a linear decrease with power (component A_2)

$$A_{EI}(\rho) = \underbrace{a \times \sqrt{\rho - \rho_c}}_{A_1} \underbrace{- b \times \left(1 + \mathrm{erf}\left(\frac{\rho - \rho_s}{\Delta\rho}\right)\right)(\rho - \rho_c)}_{A_2}$$

where ρ denotes the excitation density, and ρ_s ($\Delta\rho$) characterizes the position of the threshold (the width). The factors a and b furthermore describe the amplitudes of the two components, and ρ_c denotes the onset of the oscillation. The linear decrease in the fit ansatz was weighted by a step function to reproduce the relatively sharp transition between the two regimes. The necessity of including the step function, to properly match the experimental data, directly corresponds to the nonlinear excitation threshold. This is illustrated in Fig. 4B, where the two components of the fit are plotted separately. The behavior of A_2 shows that the linear decrease only sets in above a threshold (ρ_s). This can be understood as follows: At low excitation fluence, the nonlinear condensate-phonon coupling is not effective, but upon increasing the power, this coupling becomes exposed and dominant; the amplitude follows the transient order parameter. In this regime, the decreasing amplitude indicates the increasing photodepletion of the condensate. The depletion increases linearly with the number of photons in the pump pulse; that is, it depends linearly on the excitation density. The comparison of the two measurements at different temperatures shows that the threshold shifts to lower powers with increasing temperature, as emphasized by the two vertical lines in Fig. 4A. This also explains the previously discussed temperature dependence at the low excitation density (Fig. 3A). At low temperatures, the excitation density is below the threshold. This prevents an efficient excitation of the coupled amplitude mode. However, upon increasing the temperature, the threshold shifts to lower values, until it equals the excitation density. At this point, the coupling becomes exposed, and the amplitude of the coupled exciton-phonon system (A_{EI}) follows the order parameter.

DISCUSSION

From the temperature- and excitation density–dependent measurements, we can conclude that the 1-THz oscillation indeed results from a nonlinear coupling of the 1-THz phonon to the EI that becomes exposed at high excitation densities. Specifically, it can be described as a coupling to the order parameter of the excitonic condensate. From our measurements, we can only conclude the existence of a coupling but cannot unambiguously identify its origin. Our LDA calculations show that the 1-THz phonon modulates the Ni-Se distance (see the Supplementary Materials). Possibly as a result, the Ni 3d–Se 4p hybridization becomes modulated (*24*), which, in turn, would change the exciton onsite energies and the spatial extension of the charge transfer excitons. Figure 5 visualizes an excitation mechanism of a phonon-coupled amplitude mode. At negative time delays (Fig. 5A), no prominent coupling between the EI and phonon potential is evidenced. However, the pump

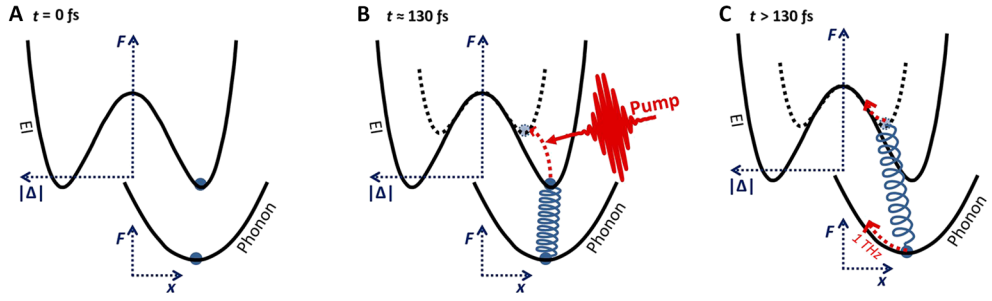

Fig. 5. Coupled EI and phonon potentials. The double-well potential represents the EI, and the single-well potential represents the phonon. Because of the strong electron-phonon coupling, a new amplitude mode emerges, which combines phonon and order parameter dynamics. The excitation mechanism can be understood as follows: (**A**) At negative time delays, no effective coupling between the potentials can be observed. (**B**) When the pump pulse arrives, it changes the potential energy landscape of EI adiabatically, that is, without exciting a Higgs amplitude mode directly. The potential shrinks, the order parameter reduces, and a coupling in the nonlinear excitation regime (represented as spring) between the EI and the phonon becomes effective. (**C**) This leads to an impulsive excitation of the 1-THz phonon because the change occurs faster than its intrinsic 1-ps response time. Coupling to the EI results in an oscillation of the coupled condensate-phonon system.

pulse (above the excitation density threshold) exposes the nonlinear coupling between EI and phonon (Fig. 5B): It depletes the exciton condensate and thus changes the potential of EI on a time scale of 130 fs, which is much longer than the 26-fs period of the Higgs mode. Because the Higgs mode's period denotes the order parameter's intrinsic response time, the order parameter can follow the changing potential adiabatically, in the sense that the order parameter always remains in the minimum of the potential and no direct excitation of a Higgs amplitude mode is possible. However, the coupled phonon has a much slower response time (1 ps) and therefore cannot follow this change adiabatically. This leads to an impulsive excitation (Fig. 5C) of the coupled order parameter–phonon system and, thus, the measured 1-THz coherent oscillations. We note that, here, the driving force of the oscillations is given by the gradient of the quenched EI potential. Therefore, that gradient (decreasing on increasing temperature) defines the temperature dependence of the oscillation amplitude [that becomes smaller on elevated temperatures (*36*)]. That behavior is distinct from the shallower coherent phonon potential at elevated temperatures (that would predict an increasing amplitude on elevated temperatures).

We further note that the peculiar effects of exciton-phonon coupling in EIs were also exposed in a recent theoretical study showing that the coupling can induce long-lived collective oscillations of an amplitude mode. Their origin stems from the phonon and from the EI intermixed electronic amplitude and phase modes (*37*).

Investigating this phonon-coupled amplitude mode allows tracing of the transient order parameter of EI at the easily accessible frequency of the phonon. The measurements at low excitation densities show that this coupling only becomes exposed above a certain threshold. This rules out a simple linear phonon excitation. In addition, the 1-THz mode's decreasing amplitude at high excitation densities is a clear indicator of a photodepletion of the excitonic condensate. We note that the excitation density dependence of the coupled mode's amplitude is independent of the electronic background signal, which shows a linear excitation density dependence running into saturation and no depletion (see the Supplementary Materials). This rules out a simple coupling of an impulsively excited coherent phonon to the electronic signal. The 1-THz mode's amplitude follows the characteristic behavior of a purely electronic Higgs-like amplitude mode. Its amplitude is proportional to the electric field of the pump pulses and decreases linearly with power at high excitation densities due to the photodepletion. This behavior points directly to the excitation mechanism of the phonon-EI–order parameter–coupled system described above.

The experimental discovery of this mode in the nonlinear excitation regime of Ta_2NiSe_5 provides a first direct fingerprint of a coherent EI ground state in the system. The collective mode's amplitude follows the system's transient order parameter as a function of excitation density and temperature. The fact that probing the phonon-coupled amplitude mode can identify a condensate is also confirmed by the behavior of the equivalent mode in Ta_2NiS_5, a material, which also shows strong excitonic binding (*27*) but no coherent condensate. In this material, the 1-THz mode shows the temperature and excitation density dependence of an uncoupled phonon (see the Supplementary Materials). This sensitivity to the coherent condensate makes the phonon-coupled amplitude mode an ideal probe to investigate the suppression of the condensate upon S-doping in $Ta_2Ni(Se_{1-x}S_x)_5$ or the BEC-BCS–like crossover within the EI phase that can be controlled in Ta_2NiSe_5 by tuning the bandgap under pressure (*26*). Beyond that, the novel scheme of probing phonon-coupled amplitude modes opens the possibility to directly investigate electronically driven phase transitions that are not accompanied by CDWs. It allows probing of the coherent amplitude response at low frequencies. This can prove useful in systems with large electronic gaps, where a direct excitation of the coherent electronic system would be very challenging because of the required extremely short time scales.

MATERIALS AND METHODS

Sample preparation

Single crystals of Ta_2NiSe_5 were grown by chemical vapor transport reaction. Elemental powders of Ta, Ni, and Se were mixed with a stoichiometric ratio and sealed into an evacuated quartz tube (~1×10^{-3} Pa) with small amount of I_2 as transport agent. The mixture was sintered in a two-zone furnace under a temperature gradient of 900°/850°C for a week. Thin strip-shaped crystals spreading in the *ac* plane were grown at the cold end of tube. The crystals were characterized by x-ray diffraction and resistivity measurements.

Pump-probe experiments

We performed the time-resolved experiments using a regenerative Ti/Sa amplifier delivering 6-μJ pulses at 800 nm with a pulse duration of 130 fs. The time-resolved reflectivity changes were measured in a degenerate pump-probe experiment at this wavelength. The pump was attenuated to obtain the desired excitation density. The size of the pump spot was 300 μm, and excitation densities of up to 1.6 mJ/cm^2 were used. Higher

excitation densities irreversibly damaged the samples. The samples were kept in an optical cryostat that allowed cooling to 80 K using liquid nitrogen and heating to 375 K.

Raman measurements

The linear Raman spectrum was measured using a Jobin Yvon Typ V 010 LabRAM single grating spectrometer, equipped with a double super razor edge filter and a Peltier-cooled charge-coupled device camera. The resolution of the spectrometer (grating, 1800 lines/mm) was 1 cm^{-1}. The spectra were taken in a quasi-backscattering geometry using the linearly polarized 632.817-nm line of a He/Ne gas laser. The power was lower than 1 mW, and the spot size was 10 µm. The scattered signal was filtered and analyzed using an additional polarizer before the spectrometer.

Phonon spectrum

To analyze the Raman spectrum and identify the oscillatory modes, we calculated the phonon spectrum at q = (0,0,0) within the density functional perturbation theory (*38*) framework using the density functional code Quantum ESPRESSO (*39*). We used projector-augmented wave pseudopotentials (*40*) from the PSLibrary v.0.3.1 (*41*), together with plane waves as a basis set, and used the LDA in the parametrization of Perdew and Zunger (*42*). The wave function (charge density) cutoff was set to 50 rydberg (Ry) (400 Ry), and a k mesh of 4 × 1 × 4 was used. The forces (<1 mRy/bohr) and the internal stress (<0.5 kbar) of the initial crystal structure (*43*) were minimized before the lattice dynamics calculation.

SUPPLEMENTARY MATERIALS

Supplementary material for this article is available at http://advances.sciencemag.org/cgi/content/full/4/3/eaap8652/DC1

section S1. Phonon spectrum of Ta_2NiSe_5 and characterization of the 1-THz phonon
section S2.1. Amplitude behavior of the 1-THz mode at low excitation densities
section S2.2. Frequency shift of the 1-THz mode
section S3. Coherent phonon: The 3-THz mode
section S4. Polarization parallel to the chains
section S5. Coherent phonon oscillation of the 1-THz mode in Ta_2NiS_5
section S6. Excitation density dependence of the electronic amplitude
fig. S1.1. Linear Raman measurements at different analyzer settings.
fig. S1.2. Real-space representation of the 1-THz A_{1g} phonon.
fig. S2.1. Amplitude of the 1-THz mode at low excitation densities.
fig. S2.2. Frequency of the phonon-coupled amplitude mode for all measurements discussed in the main text.
fig. S3. Properties of the 3-THz coherent phonon.
fig. S4. Properties parallel to the chains.
fig. S5. The 1-THz coherent phonon in Ta_2NiS_5.
fig. S6. Maximum of the electronic signal as a function of the excitation density at different temperatures.
table S1. Phonon spectrum of Ta_2NiSe_5 in the low-temperature phase at q = (0,0,0).

REFERENCES AND NOTES

1. N. F. Mott, The transition to the metallic state. *Philos. Mag.* **6**, 287–309 (1961).
2. R. S. Knox, Theory of excitons, in *Solid State Physics*, F. Seitz, D. Turnbull, Eds. (Academic Press, 1963), suppl. 5, p. 100.
3. L. V. Keldysh, Y. V. Kopaev, Possible instability of semimetallic state towards Coulomb interaction. *Sov. Phys. Solid State* **6**, 2219 (1965).
4. D. Jérome, T. M. Rice, W. Kohn, Excitonic insulator. *Phys. Rev.* **158**, 462 (1967).
5. B. I. Halperin, T. M. Rice, Possible anomalies at a semimetal-semiconductor transition. *Rev. Mod. Phys.* **40**, 755 (1968).
6. B. Zenker, D. Ihle, F. X. Bronold, H. Fehske, Electron-hole pair condensation at the semimetal-semiconductor transition: A BCS-BEC crossover scenario. *Phys. Rev. B* **85**, 121102 (2012).
7. Y. Wakisaka, T. Sudayama, K. Takubo, T. Mizokawa, N. L. Saini, M. Arita, H. Namatame, M. Taniguchi, N. Katayama, M. Nohara, H. Takagi, Photoemission spectroscopy of Ta_2NiSe_5. *J. Supercond. Nov. Magn.* **25**, 1231–1234 (2012).
8. Y. Wakisaka, T. Sudayama, K. Takubo, T. Mizokawa, M. Arita, H. Namatame, M. Taniguchi, N. Katayama, M. Nohara, H. Takagi, Excitonic insulator state in Ta_2NiSe_5 probed by photoemission spectroscopy. *Phys. Rev. Lett.* **103**, 026402 (2009).
9. H. Cercellier, C. Monney, F. Clerc, C. Battaglia, L. Despont, M. G. Garnier, H. Beck, P. Aebi, L. Patthey, H. Berger, L. Forró, Evidence for an excitonic insulator phase in 1*T*-$TiSe_2$. *Phys. Rev. Lett.* **99**, 146403 (2007).
10. S. Hellmann, T. Rohwer, M. Kalläne, K. Hanff, C. Sohrt, A. Stange, A. Carr, M. M. Murnane, H. C. Kapteyn, L. Kipp, M. Bauer, K. Rossnagel, Time-domain classification of charge-density-wave insulators. *Nat. Commun.* **3**, 1069 (2012).
11. T. Rohwer, S. Hellmann, M. Wiesenmayer, C. Sohrt, A. Stange, B. Slomski, A. Carr, Y. Liu, L. M. Avila, M. Kalläne, S. Mathias, L. Kipp, K. Rossnagel, M. Bauer, Collapse of long-range charge order tracked by time-resolved photoemission at high momenta. *Nature* **471**, 490–493 (2011).
12. J. C. Petersen, S. Kaiser, N. Dean, A. Simoncig, H. Y. Liu, A. L. Cavalieri, C. Cacho, I. C. E. Turcu, E. Springate, F. Frassetto, L. Poletto, S. S. Dhesi, H. Berger, A. Cavalleri, Clocking the melting transition of charge and lattice order in 1*T*-TaS_2 with ultrafast extreme-ultraviolet angle-resolved photoemission spectroscopy. *Phys. Rev. Lett.* **107**, 177402 (2011).
13. T. Cea, L. Benfatto, Nature and Raman signatures of the Higgs amplitude mode in the coexisting superconducting and charge-density-wave state. *Phys. Rev. B* **90**, 224515 (2014).
14. M. Eichberger, H. Schäfer, M. Krumova, M. Beyer, J. Demsar, H. Berger, G. Moriena, G. Sciaini, R. J. D. Miller, Snapshots of cooperative atomic motions in the optical suppression of charge density waves. *Nature* **468**, 799–802 (2010).
15. M. Porer, U. Leierseder, J.-M. Ménard, H. Dachraoui, L. Mouchliadis, I. E. Perakis, U. Heinzmann, J. Demsar, K. Rossnagel, R. Huber, Non-thermal separation of electronic and structural orders in a persisting charge density wave. *Nat. Mater.* **13**, 857–861 (2014).
16. T. Cea, C. Castellani, G. Seibold, L. Benfatto, Nonrelativistic dynamics of the amplitude (Higgs) mode in superconductors. *Phys. Rev. Lett.* **115**, 157002 (2015).
17. A. Tomeljak, H. Schäfer, D. Städter, M. Beyer, K. Biljakovic, J. Demsar, Dynamics of photoinduced charge-density-wave to metal phase transition in $K_{0.3}MoO_3$. *Phys. Rev. Lett.* **102**, 066404 (2009).
18. R. Matsunaga, N. Tsuji, H. Fujita, A. Sugioka, K. Makise, Y. Uzawa, H. Terai, Z. Wang, H. Aoki, R. Shimano, Light-induced collective pseudospin precession resonating with Higgs mode in a superconductor. *Science* **345**, 1145–1149 (2014).
19. R. Matsunaga, Y. I. Hamada, K. Makise Y. Uzawa, H. Terai, Z. Wang, R. Shimano, Higgs amplitude mode in the BCS superconductors $Nb_{1-x}Ti_xN$ induced by terahertz pulse excitation. *Phys. Rev. Lett.* **111**, 057002 (2013).
20. P. B. Littlewood, C. M. Varma, Amplitude collective modes in superconductors and their coupling to charge-density-waves. *Phys. Rev. B* **26**, 4883–4893 (1982)
21. D. Podolsky, A. Auerbach, D. P. Arovas, Visibility of the amplitude (Higgs) mode in condensed matter. *Phys. Rev. B.* **84**, 174522 (2011).
22. H. Y. Liu, I. Gierz, J. C. Petersen, S. Kaiser, A. Simoncig, A. L. Cavalieri, C. Cacho, I. C. E. Turcu, E. Springate, F. Frassetto, L. Poletto, S. S. Dhesi, Z.-A. Xu, T. Cuk, R. Merlin, A. Cavalleri, Possible observation of parametrically amplified coherent phasons in $K_{0.3}MoO_3$ using time-resolved extreme-ultraviolet angle-resolved photoemission spectroscopy. *Phys. Rev. B* **88**, 045104 (2013).
23. Y. Ren, G. Lüpke, Z. Xu, Photoinduced charge-density-wave dynamics in $K_{0.3}MoO_3$. *Appl. Phys. Lett.* **84**, 2169 (2004).
24. T. Taneko, T. Toriyama, T. Konishi, Y. Ohta, Orthorhombic-to-monoclinic phase transition of Ta_2NiSe_5 induced by the Bose-Einstein condensation of excitons. *Phys. Rev. B* **87**, 035121 (2013).
25. K. Seki, Y. Wakisaka, T. Kaneko, T. Toriyama, T. Konishi, T. Sudayama, N. L. Saini, M. Arita, H. Namatame, M. Taniguchi, N. Katayama, M. Nohara, H. Takagi, T. Mizokawa, Y. Ohta, Excitonic Bose-Einstein condensation in Ta_2NiSe_5 above room temperature. *Phys. Rev. B* **90**, 155116 (2014).
26. Y. F. Lu, H. Kono, T. I. Larkin, A. W. Rost, T. Takayama, A. V. Boris, B. Keimer, H. Takagi, Zero-gap semiconductor to excitonic insulator transition in Ta_2NiSe_5. *Nat. Commun.* **8**, 14408 (2017).
27. T. I. Larkin, A. N. Yaresko, D. Pröpper, K. A. Kikoin, Y. F. Lu, T. Takayama, Y.-L. Mathis, A. W. Rost, H. Takagi, B. Keimer, A. V. Boris, Giant exciton Fano resonance in quasi-one-dimensional Ta_2NiSe_5. *Phys. Rev. B* **95**, 195144 (2017).
28. S. Mor, M. Herzog, D. Golež, P. Werner, M. Eckstein, N. Katayama, M. Nohara, H. Takagi, T. Mizokawa, C. Monney, J. Stähler, Ultrafast electronic band gap control in an excitonic insulator. *Phys. Rev. Lett.* **119**, 086401 (2017).
29. Y. Murakami, P. Werner, N. Tsuji, H. Aoki, Multiple amplitude modes in strongly coupled phonon-mediated superconductors. *Phys. Rev. B.* **93**, 094509 (2016).
30. T. E. Stevens, J. Kuhl, R. Merlin, Coherent phonon generation and the two stimulated Raman tensors. *Phys. Rev. B* **65**, 144304 (2002)
31. K. Kajimura, H. Hayakawa, *Advances in Superconductivity III* (Springer, 1991).
32. O. V. Misochko, K. Kisoda, K. Sakai, S. Nakashima, Dynamics of low-frequency phonons in the $YBa_2Cu_3O_{7-x}$ superconductor studied by time- and frequency-domain spectroscopies. *Phys. Rev. B* **61**, 4305–4313 (2000).

33. B. Mansart, D. Boschetto, A. Savoia, F. Rullier-Albenque, A. Forget, D. Colson, A. Rousse, M. Marsi, Observation of a coherent optical phonon in the iron pnictide superconductor $Ba(Fe_{1-x}Co_x)_2As_2$ (x=0.06 and 0.08). *Phys. Rev. B* **80**, 172504 (2009).
34. K. Ishioka, M. Kitajima, O. V. Misochko, Temperature dependence of coherent A_{1g} and E_g phonons of bismuth. *J. Appl. Phys.* **100**, 093501 (2006).
35. K. Ishioka, M. Hase, M. Kitajima, H. Petek, Coherent optical phonons in diamond. *Appl. Phys. Lett.* **89**, 231916 (2006).
36. J. Demsar, K. Biljaković, D. Mihailovic, Single particle and collective excitations in the one-dimensional charge density wave solid $K_{0.3}MoO_3$ probed in real time by femtosecond spectroscopy. *Phys. Rev. Lett.* **83**, 800–803 (1999).
37. Y. Murakami, D. Golež, M. Eckstein, P. Werner, Photoinduced enhancement of excitonic order. *Phys. Rev. B 119*, 247601 (2017).
38. S. Baroni, S. de Gironcoli, A. Dal Corso, P. Giannozzi,Phonons and related crystal properties from density-functional perturbation theory. *Rev. Mod. Phys.* **73**, 515–562 (2001).
39. P. Giannozzi, S. Baroni, N. Bonini, M. Calandra, R. Car, C. Cavazzoni, D. Ceresoli, G. L. Chiarotti, M. Cococcioni, I. Dabo, A. Dal Corso, S. de Gironcoli, S. Fabris, G. Fratesi, R. Gebauer, U. Gerstmann, C. Gougoussis, A. Kokalj, M. Lazzeri, L. Martin-Samos, N. Marzari, F. Mauri, R. Mazzarello, S. Paolini, A. Pasquarello, L. Paulatto, C. Sbraccia, S. Scandolo, G. Sclauzero, A. P. Seitsonen, A. Smogunov, P. Umari, R. M. Wentzcovitch, QUANTUM ESPRESSO: A modular and open-source software project for quantum simulations of materials. *J. Phys. Condens. Matter* **21**, 395502 (2009).
40. P. E. Blöchl, Projector augmented-wave method. *Phys. Rev. B* **50**, 17953 (1994).
41. A. Dal Corso, Pseudopotentials periodic table: From H to Pu. *Comp. Mater. Sci.* **95**, 337–350 (2014).
42. J. P. Perdew, A. Zunger, Self-interaction correction to density-functional approximations for many-electron systems. *Phys. Rev. B* **23**, 5048–5079 (1981).
43. S. A. Sunshine, J. A. Ibers, Structure and physical properties of the new layered ternary chalcogenides tantalum nickel sulfide (Ta2NiS5) and tantalum nickel selenide (Ta2NiSe5). *Inorg. Chem.* **24**, 3611–3614 (1985).

Acknowledgments: We thank A. Schulz for measuring the linear Raman spectra. We thank T. Larkin and A. V. Boris for sharing insights from optical measurements and fruitful discussions. We also thank T. Oka, S. R. Clark, and M. Knap for the helpful comments on the topic. **Funding:** S.K. acknowledges support by the Ministerium für Wissenschaft, Forschung und Kunst Baden-Württemberg through the Juniorprofessuren-Programm and a fellowship by the Daimler und Benz Stiftung. **Author contributions:** S.K. designed and supervised the project. D.W. built the setup and measured the data with support from G.A. D.W., together with S.K., analyzed and interpreted the data with theoretical support from D.M. T.T., A.W.R., Y.L., and H.T. provided and characterized the samples and shared insight into the EI physics of the compounds. M.H. performed the calculations on the phonon spectra. All authors discussed the results. D.W. and S.K. wrote the manuscript with input and from all authors. **Competing interests:** The authors declare that they have no competing interests. **Data and materials availability:** All data needed to evaluate the conclusions in the paper are present in the paper and/or the Supplementary Materials. Additional data related to this paper may be requested from the authors.

Submitted 4 September 2017
Accepted 12 February 2018
Published 23 March 2018
10.1126/sciadv.aap8652

Citation: D. Werdehausen, T. Takayama, M. Höppner, G. Albrecht, A. W. Rost, Y. Lu, D. Manske, H. Takagi, S. Kaiser, Coherent order parameter oscillations in the ground state of the excitonic insulator Ta_2NiSe_5. *Sci. Adv.* **4**, eaap8652 (2018).

Science Advances

Coherent order parameter oscillations in the ground state of the excitonic insulator Ta_2NiSe_5

Daniel Werdehausen, Tomohiro Takayama, Marc Höppner, Gelon Albrecht, Andreas W. Rost, Yangfan Lu, Dirk Manske, Hidenori Takagi and Stefan Kaiser

Sci Adv **4** (3), eaap8652.
DOI: 10.1126/sciadv.aap8652